Chinese Chemical Letters 33 (2022) 4437–4448

Contents lists available at ScienceDirect

Chinese Chemical Letters

journal homepage: www.elsevier.com/locate/cclet

Two-dimensional transition metal chalcogenide nanomaterials for cancer diagnosis and treatment

Jingjing Wu[a,b], Tingting Hu[a], Guoping Zhao[c,*], Anran Li[b,*], Ruizheng Liang[a,*]

[a] State Key Laboratory of Chemical Resource Engineering, Beijing Advanced Innovation Center for Soft Matter Science and Engineering, Beijing University of Chemical Technology, Beijing 100029, China
[b] Beijing Advanced Innovation Center for Big Data-Based Precision Medicine, School of Engineering Medicine, Beihang University, Beijing 100191, China
[c] Department of Orthopedics, Guilin People's Hospital, Guilin 541002, China

ARTICLE INFO

Article history:
Received 27 October 2021
Revised 22 November 2021
Accepted 28 December 2021
Available online 4 January 2022

Keywords:
Two-dimensional (2D) nanomaterials
Transition metal chalcogenides (TMCs)
Synthesis method
Biomedical imaging
Cancer treatment

ABSTRACT

For more than a decade, the exfoliation of graphene and other layered materials has led to a tremendous amount of research in two-dimensional (2D) materials, among which 2D transition metal chalcogenides (TMCs) nanomaterials have attracted much attention in a wide range of applications including photoelectric devices, lithium-ion batteries, catalysis, and energy conversion and storage owing to their unique photoelectric physical properties. With such large specific surface area, strong near-infrared (NIR) absorption and abundant chemical element composition, 2D TMCs nanomaterials have become good candidates in biomedical imaging and cancer treatment. This review systematically summarizes recent progress on 2D TMCs nanomaterials, which includes their synthesis methods and applications in cancer treatment. At the end of this review, we also highlight the future prospects and challenges of 2D TMCs nanomaterials. It is expected that this work can provide the readers with a detailed overview of the synthesis of 2D TMCs and inspire more novel functional biomaterials based on 2D TMCs for cancer treatment in the future.

1. Introduction

Since the 20th century, the morbidity of cancer has been increasing year by year. Although a lot of manpower, material and financial resources have been devoted to the research of cancer treatment, cancer is still one of the serious diseases that increasingly threaten human health. Traditional cancer treatment strategies such as surgery, chemotherapy and radiotherapy (RT) are often accompanied by severe trauma, drug resistance and high recurrence rate [1–3]. Therefore, a safe and effective novel cancer treatment strategy has become a research hotspot. With the rapid development of nanoscience, it is possible to break through the aforementioned barriers with functional nanomaterials and corresponding therapeutic techniques [4–6]. For example, layered double hydroxides nanosheets (NSs), two-dimensional (2D) boron NSs and BP NSs have been proven to be effective drug-delivery platforms because of their 2D structure with large surface area [7–10]. Many nanomaterials with strong near-infrared (NIR) absorption, such as antimonene quantum dots, transition metal chalcogenides (TMCs) nanomaterials and metal oxide nanoparticles, have been shown to serve as photothermal agents for PTT of cancer [11–13]. Among them, 2D TMCs nanomaterials have attracted growing attention toward the cancer diagnosis and treatment by exploiting their fascinating chemical and physical properties.

2D TMCs nanomaterials composed of transitional metal elements typically from groups 4–7 of the periodic table (such as Mn, Fe, Nb, Mo, W and Re) and chalcogenide elements (S, Se and Te) have been extensively reported to display manifold properties such as high thermal conductivity, remarkable catalytic efficiency and distinctive optical properties [14,15]. Thus, extensive studies about their application in electrochemistry, catalysis, energy storage and biomedicine have been carried out [16–20]. In particular, due to their negligible cytotoxicity, unique structural and chemical/physical properties, 2D TMCs nanomaterials exhibit great potential in biomedical imaging and cancer treatment [21,22].

Within the bulk TMCs layers, the interactions between transitional metal atom and chalcogenide atom are covalent, and the adjacent layers are combined together by weak van der Waals forces [23–25]. This structural feature allows the bulk TMCs to be easily exfoliated into monolayers, thus revealing 2D properties. Additionally, TMCs are short of dangling bonds on their surface, thus

* Corresponding authors.
E-mail addresses: zgp96389@126.com (G. Zhao), rananli@buaa.edu.cn (A. Li), liangrz@mail.buct.edu.cn (R. Liang).

https://doi.org/10.1016/j.cclet.2021.12.080
1001-8417/

they can maintain high stability in solution and air, which is beneficial for their application in biological systems [26]. Based on their 2D structure, TMCs nanomaterials display an extremely large specific surface area, which allows them to be easily functionalized and interacted with biomedical materials to achieve improved biocompatibility and efficient loading of therapeutic agents [27,28]. Apart from their large specific surface area, 2D TMCs nanomaterials also reveal distinctive chemical and physical properties, such as optical properties, tunable electronic band structure and quantum confinement effect. For example, based on their electronic band structure and quantum confinement effect, 2D TMCs nanomaterials with thickness-dependent NIR absorption characteristics and efficient photothermal conversion properties have been explored in photothermal therapy (PTT) and photoacoustic (PA) imaging, showing advantages over synergistic diagnosis and treatment [29–31]. Moreover, the variable and tunable chemical element composition enables 2D TMCs nanomaterials with multiple or high atomic-number elements for performance optimization. For example, 2D TMCs containing multiple metal ions have been reported to result in enhanced photothermal conversion efficiency for PTT [32]. 2D TMCs with high atomic-number elements, such as W and Mo, show great potential as computed tomography (CT) imaging contrast agents and radiosensitizer for cancer diagnosis and treatment owing to their excellent X-ray attenuation properties [33–35].

Benefiting from their distinctive chemical and physical properties, 2D TMCs has been extensively studied by numerous researches. Some scientists have reviewed the preparation of 2D TMCs and their biomedical applications. For example, Chatterjee *et al.* reviewed the exfoliation and synthesis methods of 2D TMCs. Yang *et al.* summarized the application of 2D TMCs nanomaterials in drug/gene delivery and biological imaging. Gu *et al.* introduced 2D TMCs-assisted combinational therapies [36,37,21]. However, comprehensive reviews on 2D TMCs nanomaterials, which include the synthesis of 2D TMCs specifically for biomedical applications, biological imaging and cancer treatment have rarely been reported. Therefore, this review provides a focused viewpoint of the synthesis strategies of 2D TMCs nanomaterials and their biomedical application in cancer diagnosis and treatment, as shown in Fig. 1. Firstly, a detailed summary of the exfoliation and synthesis of 2D TMCs nanomaterials with good biocompatibility is provided. Secondly, a detailed introduction to their applications in biomedical imaging including magnetic resonance (MR) imaging, CT imaging, PA imaging and multimodal imaging is presented. Thirdly, recent advances in cancer treatment with 2D TMCs nanomaterials as therapeutic agents and nanocarriers are discussed. Finally, we propose the application prospects and challenges of 2D TMCs nanomaterials in cancer treatment. It is hoped that this review will shed more light on the direction of designing and synthesizing novel 2D TMCs nanomaterials to accelerate the realization of effective clinical cancer treatment in the future.

2. Synthesis of 2D TMCs nanomaterials

After Geim *et al.* successfully isolated graphene to 2D structure in 2004, the research on the preparation of nanomaterials with 2D structural features has received considerable attention and enthusiasm as well [38,39]. So far, various 2D nanomaterials have been extensively developed. Although the crystal structure and/or composition of different 2D nanomaterials vary greatly, they can still be classified into layer structured 2D nanomaterials (such as layered double hydroxides (LDHs), TMCs, hexagonal boron nitride (h-BN), graphitic carbon nitride (g-C_3N_4) and BP) and non-layer structured 2D nanomaterials (such as noble metals, metal oxides and polymers) [6,10,32,40-42]. The former possess strong covalent bonding in each layer, and the adjacent layers are stacked together by weak van der Waals interactions to form bulk materials. Whereas, the latter crystallize in three dimensions through atomic or chemical bonds to form bulk materials.

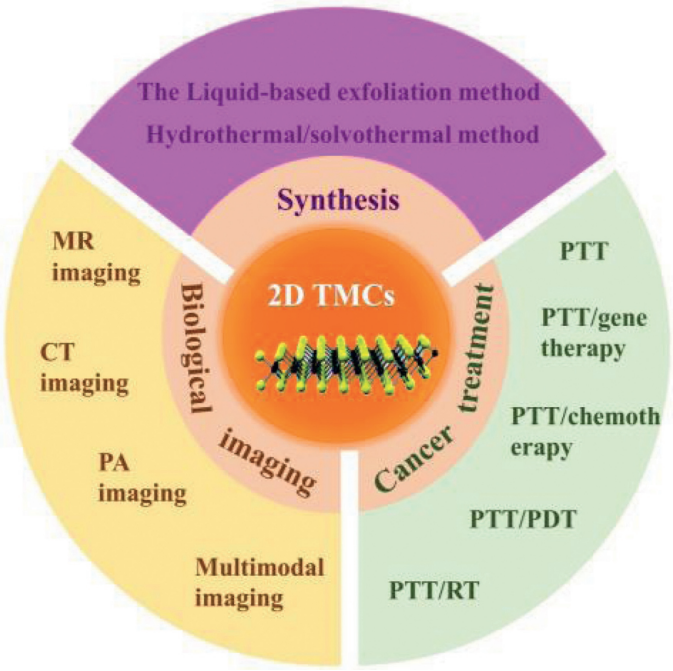

Fig. 1. Synthesis methods of 2D TMCs nanomaterials and their applications in biological imaging and cancer treatment.

For layer structured 2D nanomaterials, there are two types of mature synthesis strategies: "top-down" synthesis strategy and "down-top" synthesis strategy. "Top-down" synthesis methods, such as mechanical exfoliation and liquid-based exfoliation, destroy the weak interactions between layer structured 2D nanomaterials layers through physical or chemical force. "Down-top" synthesis methods, including chemical vapor deposition (CVD) and the hydrothermal/solvothermal method, can control the purity, particle size and chemical state of the production by regulating reaction conditions. As to non-layer structured 2D nanomaterials, most of them are synthesized by the hydrothermal/solvothermal method [43,44].

As the main subjects of this review, 2D TMCs nanomaterials should be classified as layer structured 2D nanomaterials according to previous crystal structure introduction. Therefore, the preparation of 2D TMCs nanomaterials is generally achieved by "top-down" synthesis strategies or "down-top" synthesis strategies (Table 1). Furthermore, for the effective application of 2D TMCs nanomaterials in cancer diagnosis and treatment, it is necessary for them to possess suitable size, good biocompatibility and low toxicity. 2D TMCs prepared by mechanical exfoliation and CVD are generally large-sized and water insoluble, thus are unsuitable for biological applications, especially for *in vivo* treatments [45–47]. By contrast, 2D TMCs prepared by the liquid-based exfoliation method or hydrothermal/solvothermal method are well-sized and highly stable [48–53]. For this reason, we will focus on the latter two strategies in this section.

2.1. The liquid-based exfoliation method

2.1.1. Solvent-assisted exfoliation

Solvent-assisted exfoliation generally refers to the destruction of the bulk TMCs interlayer interactions by using organic solvents with the assistance of ultrasonic or shearing force, thus achieving the separation of TMCs layers. In this process, the solvent

Table 1
Currently mature preparation methods of 2D TMCs nanomaterials and their advantages and disadvantages are summarized.

Strategy	Synthesis methods	Subsynthesis methods	Representative materials	Advantage	Disadvantage	Ref.
"Top-down" synthesis strategy	Mechanical exfoliation	Including the scotch tape method, micromechanical cleavage	MoS_2, $NbSe_2$	High quality	Large size, low yield	[45,46]
	Liquid-based exfoliation	Solvent-assisted exfoliation	MoS_2, WS_2	Excellent biocompatibility, high stability	The destroyed crystal structure	[55,56]
		Surfactant/stabilizer-assisted exfoliation	MoS_2	Good dispersibility, satisfactory size	The destroyed crystal structure	[57–60]
		Chemical-assisted intercalation and exfoliation	MoS_2, WS_2	High stability, excellent dispersibility	Rigid and complex reaction requirement, hard-to-control intercalation extent	[69,71]
		Electrochemical intercalation and exfoliation	2H-MoS_2, ZrS_2 and $MoSe_2$	Easy functionalization, high stability	Special equipment and technology requirement	[72,73]
"Down-top" synthesis strategy	Chemical vapor deposition (CVD)	–	MoS_2	Thickness controllable, high quality	Large size, water insoluble	[31]
	Hydrothermal/ solvothermal method	–	CoFeMn dichalcogenide (CFMS), MoS_2 and ReS_2	Satisfactory size, high stability	Rigid reaction conditions requirement	[32,75,79]

molecules can weaken the interactions between adjacent layers of bulk TMCs, while the ultrasonication allows them to be easily thinned to fewer layers or even single layers. Based on this, Coleman *et al.* proposed a direct liquid-based exfoliation method to prepare 2D TMCs nanomaterials in 2011 [54]. It has been found that bulk TMCs, such as WS_2, MoS_2, $MoSe_2$ and $MoTe_2$, can be effectively exfoliated into 2D nanomaterials directly by ultrasonication in appropriate solvents, such as isopropanol, dimethylformamide and *N*-methyl-pyrrolidone (NMP). It should be pointed out that the crystal structure of 2D TMCs nanomaterials obtained by this method is generally destroyed by ultrasonic or shearing force, which will have a certain impact on their photoelectric properties. Nevertheless, this synthesis method is still a fascinating exfoliating strategy owing to its satisfactory size and good dispersibility. Since then, the exfoliation of bulk TMCs in different solvents has been extensively studied. For example, Zhao *et al.* reported an improved oleum-treated liquid exfoliation method that successfully prepared MoS_2 NSs with a grinding step and high temperature (Fig. 2a) [55]. Pérez *et al.* reported a one-step liquid phase exfoliation strategy to prepare MoS_2 and WS_2 NSs which were successfully exfoliated in NMP or isopropanol/water mixtures using mild bath ultrasonication at controlled temperature [56]. The prepared ultrathin NSs were incubated with human breast cancer cells to demonstrate their good biocompatibility for future biomedical applications.

2.1.2. Surfactant/stabilizer-assisted exfoliation

Apart from solvents, surfactants/stabilizers have also been explored as exfoliating agents to obtain aqueous dispersion of surface modified or functionalized TMCs NSs to facilitate their further applications in biomedical systems [57,58]. Thus, various surfactants and stabilizers have been utilized to promote the exfoliation of TMCs nanomaterials. For example, De *et al.* reported a facile strategy to prepare functionalized 2H-MoS_2 NSs in a thiol surfactant within a short period of time [59]. The as-prepared 2H-MoS_2 NSs functionalized with thiol ligands was demonstrated to be considerably stable for an extended period of time (> 8 months) without apparent restacking under ambient conditions. Moreover, these 2H-MoS_2 NSs have been proved to possess good hemocompatibility, which enables the *in vivo* application of 2D TMCs nanomaterials. In addition, Zhang *et al.* successfully prepared high-quality 2D MoS_2 NSs through polyphenol-assisted aqueous exfoliation (Fig. 2b) [60]. In this process, polyphenols, as a class of superior water-soluble stabilizers, could quickly and effectively realize the preparation of MoS_2 NSs under optimized conditions.

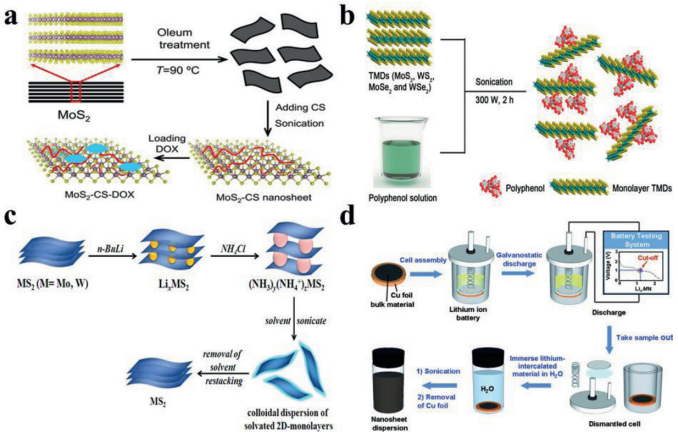

Fig. 2. The liquid-based exfoliation method of 2D TMCs nanomaterials: (a) Scheme illustration of the high-throughput synthesis of MoS_2-CS NSs. Reproduced with permission [55]. Copyright 2014, American Chemical Society. (b) The polyphenol-assisted aqueous exfoliation process of TMDs under sonication. Reproduced with permission [60]. Copyright 2018, American Chemical Society. (c) Schematic illustration of the steps involved in the synthesis, exfoliation and restacking of ammoniated MS_2 (M = Mo, W). Reproduced with permission [71]. Copyright 2014, American Chemical Society. (d) The electrochemical lithium intercalation process to produce 2D NSs from the layered bulk material (MN = BN, metal selenides, or metal tellurides in Li_xMN). Reproduced with permission [72]. Copyright 2012, Wiley-VCH Verlag GmbH & Co. KGaA, Weinheim.

The exfoliated MoS_2 NSs were demonstrated to possess excellent biocompatibility, high stability and strong NIR adsorption, making them promising agents for efficient PTT.

2.1.3. Chemical-assisted intercalation and exfoliation

Chemical-assisted intercalation and exfoliation method, as one of the most advanced preparation methods, inserts molecules or ions into bulk TMCs layers in liquid and then exfoliates them with ultrasonication to prepare 2D TMCs for application in biosystems [61]. Among them, alkali metals (Na, K and Li) have been widely explored as intercalating agents for the intercalation of bulk TMCs [62–68]. For example, Morrison *et al.* successfully prepared MoS_2 NSs using Li-intercalation and ultrasonication [69]. The toxicity evaluation revealed that MoS_2 NSs exfoliated with methyllithium possess better biocompatibility than those exfoliated with *n*-butyllithium- and *tert*–butyllithium, which enlightens

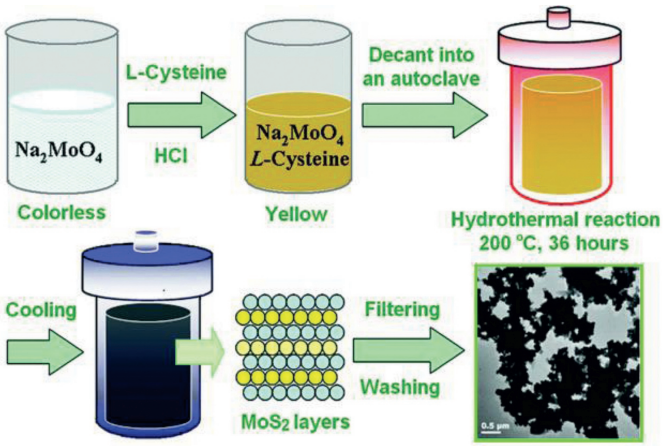

Fig. 3. The preparation of MoS_2 by a simple hydrothermal method. Reproduced with permission [74]. Copyright 2015, Royal Society of Chemistry.

us to choose optimal intercalating agents to exfoliate bulk TMCs nanomaterials for biomedical applications [70].

In addition to alkali metals, small molecules with low toxicity have also been utilized as intercalating agents. For example, Jeffery *et al.* prepared MS_2 (M = Mo and W) NSs through NH_3/NH_4^+-intercalation and subsequent exfoliation with ultrasonication (Fig. 2c) [71]. The resultant MS_2 NSs exhibit high stability and excellent dispersibility in a variety of solvents, making them promising candidates for biomedical applications. Although this method is attractive, there are still problems such as the rigid and complex reaction requirement and hard-to-control intercalation extent.

2.1.4. Electrochemical intercalation and exfoliation

The chemical Li-intercalation and exfoliation method has been extensively applied to the successful preparation of 2D TMCs NSs, but its practical application is often limited by long reaction time and harsh reaction conditions. To address these problems, Zhang *et al.* developed an efficient electrochemical Li-intercalation and exfoliation method to prepare TMCs NSs (Fig. 2d) [72]. By precisely controlling the intercalation degree of Li ions, and then transferring the well-intercalated nanomaterials to water or ethanol solution for ultrasonication, TMCs NSs with a high yield and excellent quality could be obtained. Since then, more 2D TMCs nanomaterials, including MoS_2, WS_2, ZrS_2, $MoSe_2$ and WSe_2, has been easily obtained using this method. In addition to Li-intercalation, sodium intercalation in 2H-MoS_2 has also been reported for electrochemically exfoliated preparation of MoS_2 NSs [73]. Due to their high stability and easy functionalization, these TMCs NSs prepared by the electrochemical intercalation and exfoliation method show great promise in the biomedicine field.

2.2. Hydrothermal/solvothermal method

Hydrothermal/solvothermal method has attracted much attention because of its ability to prepare TMCs NSs with ideal size and thickness. This method employs metal salts as the precursors, which are chemically reacted in sealed Teflon-lined autoclaves at reaction temperatures above 100 °C to synthesize TMC NSs (Fig. 3) [74]. As a representative example of the hydrothermal method, Shi *et al.* reported an efficient and versatile one-pot strategy for the preparation of PEGylated MoS_2 NSs by applying $(NH_4)_2MoS_4$ as the precursor [75]. The employed PEG chain was effectively anchored on the synthesized MoS_2 NSs. This surface modification with PEG was conducive to the controllable preparation of NSs and endowed them with excellent stability and favorable biocompatibility. However, this one-pot strategy still has such disadvantages as uncontrollable number of MoS_2 layers and requirement for high pressure in the synthesis process. Recently, Liang *et al.* proposed a new hydrothermal method to prepare TMCs NSs [32,76-78]. Using ultrathin LDHs NSs containing different transition metal elements (Co, Fe, Mn, Cu) as the precursor, the TMCs NSs with uniform size were achieved *via* a simple *in situ* selenylation or vulcanization reaction. Moreover, *in vitro* and *in vivo* experiments demonstrated that the prepared TMCs NSs have great potential to serve as a nanoplatform for efficient cancer treatment.

Different from the hydrothermal method which generally utilizes aqueous solution as the reaction medium, the solvothermal method utilizes organic solvents to synthesize TMCs NSs at a higher temperature due to the boiling point of organic solvents. The synthesis can proceed automatically under high pressure when the required temperature is reached. Shen *et al.* successfully synthesized uniform ReS_2 NSs in oleylamine by the use of $NaReO_4$ and S [79]. The resultant ReS_2 NSs exhibited high NIR absorption performance, strong X-ray attenuation and good biocompatibility *in vivo*, demonstrating their potential application in cancer imaging and therapy. By adjusting different experimental parameters, various 2D TMCs with desirable structural and physical and chemical properties can be acquired by using this preparation strategy [80–82]. However, the rigidity of experimental conditions typically from high reaction temperature and high reaction pressure restrict its application.

3. Biological imaging of 2D TMCs nanomaterials

As a guideline for *in vivo* therapy, biological imaging has been widely exploited to monitor the intracellular transport of therapeutic agents in real time and foresee the therapeutic outcomes [83]. Currently, the dominant biological imaging techniques in cancer treatment include MR imaging, CT imaging and PA imaging, which have been greatly improved with the rapid development of nanoscience and technology. Compared with other nanomaterials, 2D TMCs have emerged as potential candidates for biological imaging because of their attractive optical/electrical/magnetic properties and relatively facile preparation process. In this section, the application of TMCs NSs as contrast agents in MR imaging, CT imaging, PA imaging and multimodal imaging will be discussed.

3.1. MR imaging

MR imaging is an ideal approach for noninvasive longitudinal studies because it require no ionization radiation and has no limitation on the depth of penetration, and the high temporal and spatial resolution makes it particularly suitable for tumor imaging application [84]. A variety of 2D TMCs nanomaterials with magnetic property have been developed to achieve superior MR imaging. For example, Liu *et al.* synthesized FeS nanoplates *via* a simple one-step approach followed by surface modification with PEG to achieve good biocompatibility [85]. The resultant PEGylated FeS (FeS-PEG) nanoplates displayed strong magnetic property. The corresponding T_2 relaxation efficiency (r_2) of FeS-PEG nanomaterials is 209.8 L $mmol^{-1}$ s^{-1}, which is dramatically higher than those of the commercial T_2 contrast agents such as ferumoxsil, ferrixan and ferumoxide, whose r_2 are 72 L $mmol^{-1}$ s^{-1}, 151 L $mmol^{-1}$ s^{-1} and 98.3 L $mmol^{-1}$ s^{-1}, respectively. After 4T1 tumor-bearing mice were intravenously injected with FeS-PEG, significant T_2-weighted MR imaging signals were observed at the tumor site. Similarly, Liang *et al.* prepared CoFe-selenide (CFS) NSs *via* a simple *in situ* selenylation method and modified them with PEG to generate CFS-PEG, displaying a satisfactory T_2-weighted MR imaging capability

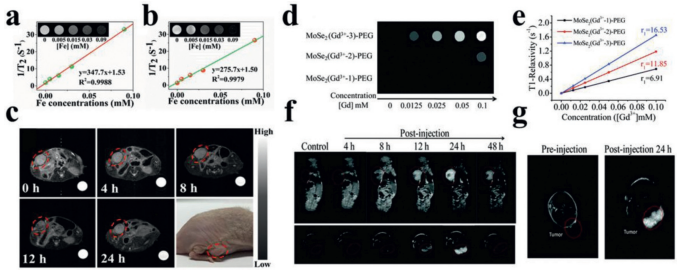

Fig. 4. T_2-weighted relaxivity and MR images (inset) of (a) CFS-PEG NSs and (b) CoFe-LDH NSs with various Fe concentrations. (c) *In vivo* MR imaging of Hela tumor-bearing nude mouse with intravenous injection of CFS-PEG NSs at various time points. Reproduced with permission [77]. Copyright 2020, American Chemical Society. (d) T_1-weighted MR images and (e) T_1 efficiency of three types of $MoSe_2$ (Gd^{3+})-PEG at different concentrations. (f) MR imaging of a cross section (the upper row) and longitudinal section (the bottom row) obtained from tumors of mice at different time intervals after *i.v.* injection of $MoSe_2$ (Gd^{3+})-PEG. (g) T_1-Weighted MR images of mice before and 24 h after *i.v* injection with $MoSe_2$ (Gd^{3+})-PEG. Reproduced with permission [86]. Copyright 2018, Royal Society of Chemistry.

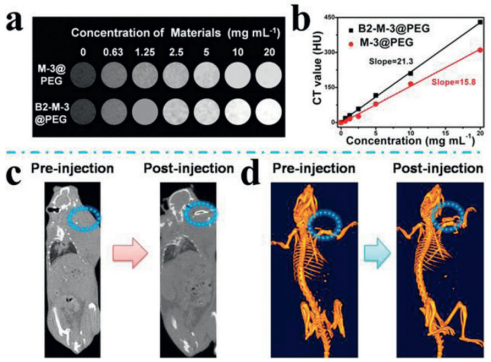

Fig. 5. (a) *In vitro* CT images of M-3@PEG and B2-M-3@PEG at different concentrations. (b) HU value of B2-M-3@PEG aqueous solution as a function of the concentration. (c), (d) CT imaging and 3D renderings of CT images of a tumor-bearing mouse: pre- and post-injection *in situ*. Reproduced with permission [94]. Copyright 2019, Elsevier Ltd.

with a large r_2 value, calculated to be 347.7 L $mmol^{-1}$ s^{-1} (Figs. 4a-c) [77]. After intravenous injection of CFS-PEG NSs, prominent signal intensity of MR imaging at the tumor site was observed at 12 h post-injection.

To endow more 2D TMCs nanomaterials applied in MR imaging, magnetic metal ions such as Fe^{3+}, Co^{3+}, Ni^{2+}, Mn^{2+} and Gd^{3+} were doped into the sandwich structure of TMCs NSs. For example, Liu *et al.* synthesized Gd^{3+}-doped $MoSe_2$ NSs by a simple liquid-phase method and modified them with PEG (Figs. 4d-g) [86]. The prepared $MoSe_2$ (Gd^{3+})-PEG sample displayed strong T_1-weighted MR imaging capacity owing to the doped Gd^{3+} with seven unpaired electrons and high magnetic moment characteristics. The T_1 relaxation efficiency of the sample obviously enhances with the increase of paramagnetic Gd^{3+} doping ratio. When the Mo: Gd feed ratio was 70:10, the T_1 relaxation efficiency (r_1) of $MoSe_2$ (Gd^{3+})-PEG was 16.53 L $mmol^{-1}$ s^{-1}, which was dramatically higher than that of gadopentetate dimeglumine (4.29 L $mmol^{-1}$ s^{-1}). Subsequently, *in vivo* experiments further verified $MoSe_2$ (Gd^{3+})-PEG nanomaterials' excellent MR imaging performance in mice bearing HepG2 tumors, and the signal intensity of corresponding MR imaging at tumor sites was distinctly increased by about six times compared with that before injection.

3.2. CT imaging

Unlike MR imaging, which relies much on magnetic property of TMCs NSs, CT imaging requires the TMCs NSs to possess high atomic number elements (such as Mo and W) and high X-ray absorption coefficients [87–89]. Zhao *et al.* and Yang *et al.* fabricated 2D WS_2 NSs modified with bovine serum albumin (BSA) and PEG with stronger signals than the clinically approved contrast agents such as iopromide and iohexol, and thus indicating potential as CT imaging contrast agents for practical tumor diagnosis [90,91]. Similarly, Shen *et al.* fabricated 0D/2D/0D sandwich heterojunctions to realize CT imaging-guided tumor ablation by assembling 0D N-doped carbon dots onto 2D structure of MoS_2 NSs [92].

To improve the stability and clarity of CT imaging, Chen *et al.* reported a feasible one-pot strategy to prepare MoS_2/Bi_2S_3-PEG (MBP) NSs [93]. Bi_2S_3 with satisfactory X-ray attenuation coefficient and strong radiosensitization effect endowed the prepared MBP composite NSs with superior CT imaging capability and drastic radiation enhancement effect during tumor diagnosis and treatment. MoS_2 also endowed the composite NSs with outstanding PTT effect. *In vivo* experiments verified that MBP composite NSs can achieve biological imaging-guided effective cancer treatment. Later, Qu *et al.* constructed $MoSe_2/Bi_2Se_3$ NSs *via* a cation-exchange strategy (Fig. 5) [94]. The obtained $MoSe_2/Bi_2Se_3$ nanoheterostructures exhibited higher CT imaging contrast than $MoSe_2$ sample, which is due to the higher X-ray absorption coefficient of Bi element. Moreover, these nanoheterostructures integrated CT imaging and multimodal therapy into one nanoplatform, which is expected to provide a possibility for future clinical biomedical imaging-guided treatment.

3.3. PA imaging

As a novel biomedical imaging technology with non-invasive and non-ionizing radiation characteristics, PA imaging has the advantages of high selectivity and deep penetrability which helps to obtain the required tissue images with high resolution and strong contrast [95,96]. The photothermal efficacy of nanomaterials is usually utilized in PA imaging to generate thermal signals through thermal expansion or bubble formation. The continuous generation of air microbubbles greatly improves the resolution of PA imaging [97]. Various nanomaterials with strong photothermal efficacy have been extensively explored as exogenous PA imaging contrast agents for tumor diagnosis. Among them, 2D TMCs nanomaterials are considered as ideal PA imaging contrast agents due to their satisfactory photothermal conversion efficiency and excellent biocompatibility. For example, Zheng *et al.* successfully synthesized single-layer (S-MoS_2), few-layer (F-MoS_2), and multi-layer (M-MoS_2) NSs without further surface functionalization by using albumin-assisted layer-by-layer exfoliation strategy [35]. Among these three kinds of NSs, S-MoS_2 NSs showed the best NIR absorption and satisfactory PA contrast performance. After the mice were injected with S-MoS_2, F-MoS_2 and M-MoS_2 samples, respectively, the PA signal intensity produced by the S-MoS_2 group is higher than that of the F-MoS_2 and M-MoS_2 groups, indicating the great potential of S-MoS_2 in sensitive PA imaging. Subsequently, Liang *et al.* prepared ultrathin PEGylated CoCuFe-selenide (CCFS-PEG) NSs and polyvinyl pyrrolidone (PVP) modified CoFeMn dichalcogenide (CFMS-PVP) NSs for PA imaging and multimodal therapy (Fig. 6) [76,32]. The synthesized CFS-PEG and CFMS-PVP were demonstrated to possess excellent PA imaging effect and ultralow limit of detection.

To further improve the sensitivity of PA imaging, the integration of TMCs NSs with other materials has been explored. For example, Kang *et al.* successfully fabricated methoxy–polyethylene glycol-*co*-polypyrrole copolymer (mPEG-*co*-PPyr) and mPEG-co-PPyr/MoS_2 composite [98]. It has been showed that both of the nanomaterials can absorb optical energy and transfer it into thermal or PA signals. However, compared with mPEG-*co*-PPyr,

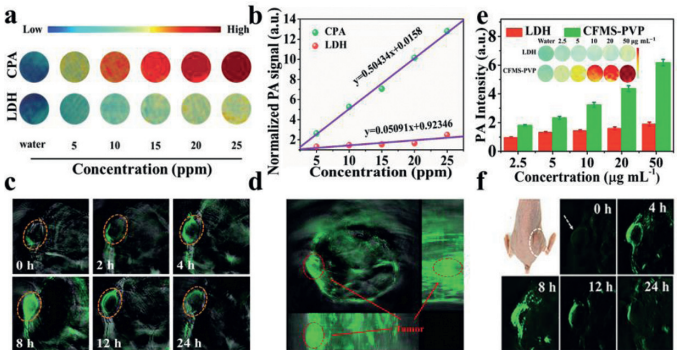

Fig. 6. (a) PA images and (b) PA intensity of CoCuFe-LDH and CPA aqueous suspensions with various concentrations. (c) *In vivo* PA imaging of the tumor (highlighted by a red circle) at various time points after the mouse was intravenously injected with CPA. (d) A 3D PA image of tumor at 8 h post-injection, based on image reconstruction. Reproduced with permission [76]. Copyright 2021, Elsevier Ltd. (e) PA intensity of CFMS-PVP NSs and CoFeMn-LDH aqueous suspension at various concentrations. (f) Multispectral optical tomography system (MSOT) images of tumor tissue (arrows) at different time points after injection *via* the tail vein. Reproduced with permission [32]. Copyright 2020, Wiley-VCH Verlag GmbH & Co. KGaA, Weinheim.

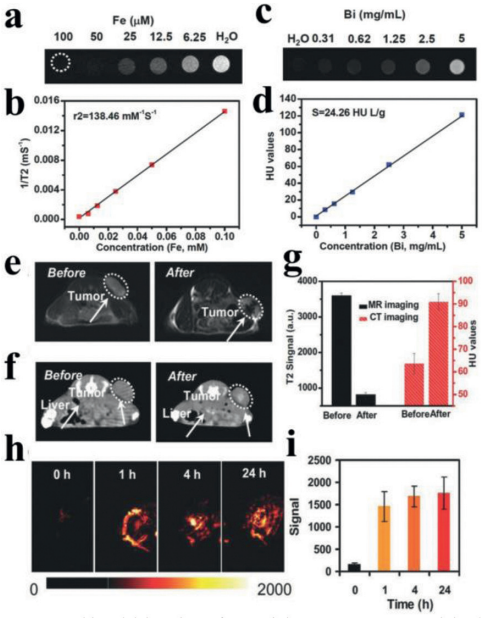

Fig. 7. Multimodal imaging of $FeSe_2/Bi_2Se_3$-PEG. (a) T_2 weighted MR images and (b) T_2 relaxation rates of $FeSe_2/Bi_2Se_3$-PEG solutions with different concentrations. (c) CT images and (d) HU values of $FeSe_2/Bi_2Se_3$-PEG solutions with different concentrations. (e) T_2-weighted MR images of mice before and 24 h after *i.v.* injection with $FeSe_2/Bi_2Se_3$-PEG. (f) *In vivo* CT images of mice before and 24 h after *i.v.* injection with $FeSe_2/Bi_2Se_3$-PEG. (g) Quantified MR and CT signals of tumors from mice before and 24 h after *i.v.* injection of $FeSe_2/Bi_2Se_3$-PEG based on the above imaging data. (h) *In vivo* PA images of tumors from mice after injection with $FeSe_2/Bi_2Se_3$-PEG, taken at different time points. (i) Quantified PA signals of tumors from mice after *i.v.* injection of $FeSe_2/Bi_2Se_3$-PEG. Reproduced with permission [103]. Copyright 2016, Wiley-VCH Verlag GmbH & Co. KGaA, Weinheim.

mPEG-*co*-PPyr/MoS_2 composite have higher PA signal amplitude under 700 nm NIR laser irradiation. It is speculated that the better PA activity of mPEG-*co*-PPyr/MoS_2 composite was due to the heterogeneous interfacial contact between mPEG-co-PPyr and MoS_2 NSs after integration. Laser irradiation of MoS_2 might increase the local temperature of mPEG-co-PPyr/MoS_2 composite and promote their thermal conductive transfer to amplify PA signal. With such distinct optical properties and a tendency to convert thermal input into PA signals, this nanocomposite is expected to be a promising PA contrast agent.

3.4. Multimodal imaging

Biomedical imaging has become the cornerstone of modern oncology. To obtain faster, more accurate and robust diagnosis, nanomaterials with multimodal imaging performance have been widely explored to guide the treatment of tumors [99–101]. Benefiting from the distinct structural features, variable element composition and favorable chemical/physical properties, 2D TMCs nanomaterials have thus become an attractive class of nanomaterials and they have broad prospects in multimodal imaging. For example, Cheng *et al.* synthesized various types of metal ions (such as Fe^{3+}, Co^{3+}, Ni^{2+}, Mn^{2+} and Gd^{3+})-doped WS_2 NSs using the unique sandwich structure of 2D TMCs [81]. The Gd^{3+}-doped WS_2 (WS_2:Gd^{3+}) NSs were chosen as a representative example to accomplish trimodal PA/CT/MR imaging-guided combined PTT and RT.

In addition to the ion-doped approach, multimodal imaging can also be achieved by integrating other functional nanomaterials into one nanoplatform. For example, Zhao *et al.* constructed MoS_2/Fe_3O_4 (MSIOs) nanocomposites by integrating MoS_2 (MS) NSs and Fe_3O_4 (IO) nanoparticles for dual-modal MR/PA imaging-guided magnetic targeting PTT [102]. Liu *et al.* prepared $FeSe_2$ decorated Bi_2Se_3 ($FeSe_2/Bi_2Se_3$) NSs by a cation exchange method and then functionalized them with PEG (Fig. 7) [103]. The resultant $FeSe_2/Bi_2Se_3$-PEG nanomaterials were labeled with radioisotope ^{64}Cu by using a chelate-free strategy to fabricate ^{64}Cu-$FeSe_2/Bi_2Se_3$-PEG. The strong magnetic property of $FeSe_2$, large X-ray attenuation coefficient of Bi_2Se_3, high NIR absorption of the whole nanostructures, and chelation of radioisotope ^{64}Cu enable ^{64}Cu-$FeSe_2/Bi_2Se_3$-PEG to achieve tetra-modal MR/CT/PA/PET imaging-guided synergistic PTT/RT therapy. These examples forcefully confirmed that 2D TMCs nanomaterials have great prospect in biological imaging and can be a feasible platform for image-guided cancer treatment.

4. Cancer treatment of 2D TMCs nanomaterials

The development of highly efficient anticancer strategy is urgent since cancer remains one of the most serious threats to human health and life. Up to now, large numbers of nanomaterials have been reported for cancer-therapeutic applications [104]. Among them, 2D TMCs nanomaterials with unique structural features, variable chemical element composition and strong NIR absorption have emerged as potential candidates for applications in cancer treatment [105]. In this section, we will comprehensively discuss the application of 2D TMCs nanomaterials as therapeutic agents and nanocarriers in cancer treatment, including PTT, combination of PTT with gene therapy, combination of PTT with chemotherapy, combination of PTT with photodynamic therapy (PDT), and combination of PTT with RT.

4.1. PTT

Compared with traditional treatments, PTT is a promising therapeutic method with the advantages of minimal invasiveness, high regional selectivity and low toxicity [106]. PTT generally utilizes photothermal agents to convert light energy into hyperthermia within the tumor tissue under the irradiation of external NIR laser for tumor ablation [107–109]. Thus, the rational design and synthesis of high-efficiency photothermal agents is crucial to the satisfactory performance of PTT [29,110-112]. With the rapid development of nanoscience, PTT based on the unique chemical/physical properties of nanomaterials has attracted more and more attention. Researchers have established 2D TMCs nanomaterials systems for PTT

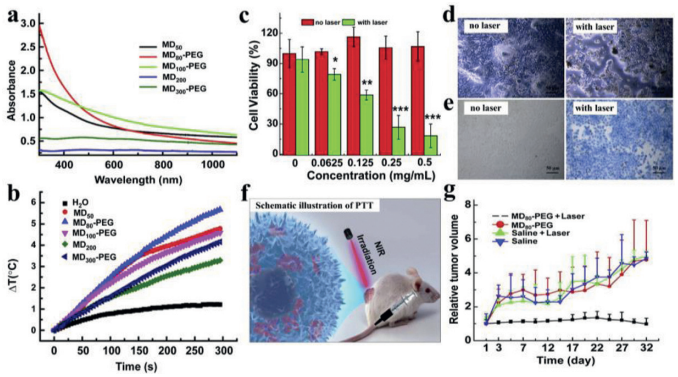

Fig. 8. (a) UV–vis–NIR spectra of different MoS_2 aqueous dispersions as noted ([Mo] =40 μg/mL). (b) Temperature profiles of water and different MoS_2 aqueous dispersions at Mo concentration of 100 μg/mL with time (0–300 s) under 808 nm laser at the power density of 0.6 W/cm^2. (c) Cell viability assay of 4T1 cells after treated with or without 808 nm NIR laser (5 min, 1 W/cm^2), cells were pre-incubated with MD_{80}-PEG (0.5 mg/mL) for 4 h before laser irradiating. (d) Show the phase-contrast photomicrographs of 4T1 cells (pre-incubated with 0.5 mg/mL of MD_{80}-PEG for 4 h) without or with laser irradiating, respectively. (e) Are the corresponding trypan blue staining results of (d). (f) Schematic illustration of PTT, mouse was intravenously injected with MD_{80}-PEG dispersion and irradiated with NIR laser. (g) The growth profile of 4T1 xenografted tumors after various treatments as indicted. Reproduced with permission [113]. Copyright 2014, Elsevier Ltd.

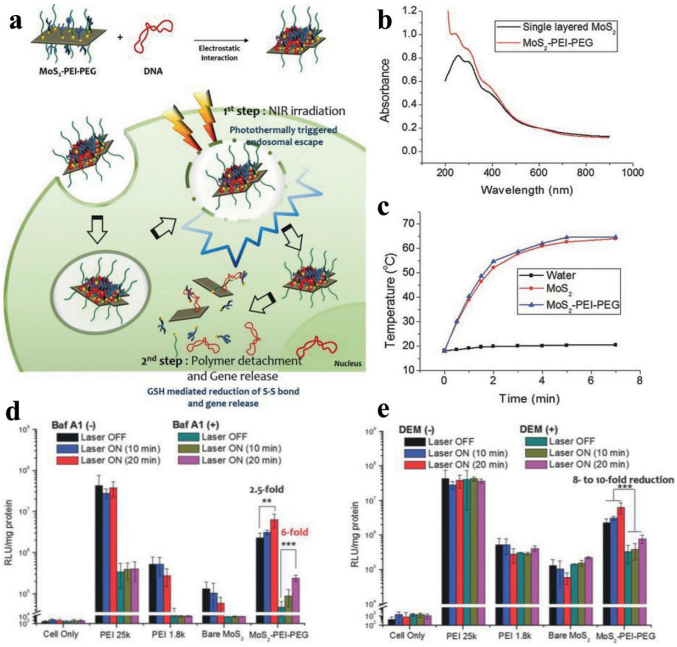

Fig. 9. (a) Schematic illustration of sequential plasmid DNA delivery using MoS_2-PEI-PEG nanocomposite by photothermally triggered endosomal escape followed by redox-mediated polymer detachment and DNA release. (b) Absorbance spectra of MoS_2 and MoS_2-PEI-PEG. (c) Photothermal effect of MoS_2 and MoS_2-PEI-PEG with 808 nm laser irradiation at the power density of 4 W/cm^2. Luciferase reporter gene expression assay after (d) Baf A1 treatment and (e) DEM treatment to inhibit proton sponge effect and glutathione activity, respectively in HCT116 at N/P ratio of 10. Reproduced with permission [122]. Copyright 2015, Wiley-VCH Verlag GmbH & Co. KGaA, Weinheim.

by virtue of their strong NIR absorption. For example, PEGylated MoS_2 (MoS_2-PEG) NSs with controllable particulate size were successfully fabricated by Wang *et al.* using a solvothermal method (Fig. 8) [113]. They found that the prepared NSs exhibited optimized photothermal conversion performance by modulating the particulate diameter and further surface PEGylation. The optimized MoS_2-PEG NSs under 808 nm laser irradiation showed promising anti-cancer efficacy without hemolysis, coagulation and toxicity *in vitro* and *in vivo*. Fu *et al.* thereafter reported that the interlayer-expanded MoS_2 (E-MoS_2) NSs displayed higher photothermal conversion efficiency with 808 nm laser irradiation than the MoS_2 NSs with normal interlayer distance [114]. *In vitro* and *in vivo* results further validated that E-MoS_2 NSs are promising photothermal agents for more efficient tumor ablation.

The above studies mainly focused on the design and development of photothermal agents with strong light absorption in NIR-I window (650–1000 nm). However, considering that the biological tissue is a highly scattering medium, the tissue penetration depth is only about 1 cm when utilizing NIR-I laser, which cannot satisfy demand for the translational study of PTT. Recently, a novel NIR-II window therapeutic studies with wavelengths ranging from 1000 nm to 1700 nm have been confirmed the enhanced therapeutic efficacy of PTT compared with NIR-I window owing to the deeper depth of tissue penetration and higher maximum permissible exposure (MPE) to the laser [115–118]. For example, Liang *et al.* prepared ultrathin $CuFe_2S_3$ NSs *via* a facile hydrothermal method [78]. After modification with PEG, the PEGylated $CuFe_2S_3$ NSs ($CuFe_2S_3$-PEG) with high NIR-II absorption and remarkable photothermal conversion efficiency at 1064 nm were acquired. *In vitro* and *in vivo* anti-tumor studies certified that the resultant $CuFe_2S_3$-PEG with 1064 nm laser irradiation has remarkable PTT effect. These results certified that $CuFe_2S_3$-PEG could be employed as a high-efficiency photothermal agent for future cancer treatment. However, although the photothermal therapeutic potential of some 2D TMCs nanomaterials has been recognized by some pioneering studies, the exploration of novel 2D TMCs nanomaterials with the ability to accurately control heating sites and rates is still in process.

4.2. Combination of PTT with gene therapy

Gene therapy involves introducing certain genetic materials (such as DNA, small interfering RNA (siRNA) and oligonucleotides) as therapeutic drugs into the patient's cells to cure diseases by compensating for abnormal genes, generating beneficial proteins or regulating the immune system [119,120]. However, the fragile structure of these therapeutic genetic materials makes the therapy less effective. Thus, an effective gene delivery carrier becomes a primary issue. Benefiting from their excellent biocompatibility, unique physicochemical properties and easy modification, nano-sized nonviral carriers have attracted tremendous attention in gene therapy. Among them, 2D TMCs with large surface areas and excellent biocompatibility have emerged as promising candidates for gene therapy. It is reported that Guo *et al.* developed well-surface modified MoS_2 as 2D gene delivery carriers for cancer treatment [121]. After modification with lipoic acid-modified polyethylene glycol (LA-PEG) and branched polyethyleneimine (PEI), the obtained positively charged MoS_2-PEG-PEI could be used as nanomaterial carriers of siRNA to realize the knockdown of Polo-like kinase 1 (PLK1), a proverbial oncogene. *In vitro* experiments revealed that the optimal gene knockdown and significant cancer cell apoptosis were realized by utilizing 2D MoS_2 as nanocarriers for PLK1 silencing.

The second pivotal issue is that the prepared 2D TMCs-gene nanomaterials can effectively escape from the endosome and release the therapeutic genetic materials. It has been reported that 2D TMCs NSs with strong NIR absorption can convert NIR light into hyperpyrexia, thus stimulating the escape and release of genes. As a paradigm, Kim *et al.* fabricated MoS_2-PEI-PEG as nanocarriers to load DNA by electrostatic interaction, thus forming nanocomposites with fairly high stability (Fig. 9) [122]. Various blocking assays in the cellular model system have elucidated that the prepared nano-

sized complex could achieve the endosomal escape triggered by local hyperpyrexia and subsequent gene release triggered by internal stimulation to remarkably improve gene delivery efficiency without severe cytotoxicity. In another study, Yong *et al.* combined MoS_2 NSs functionalized with folic acid (FA)-PEG polymers and polyallylamine hydrochloride (PAH) with siRNAs [123]. A multi-gene delivery platform based on the surface functionalized 2D MoS_2 NSs was designed, which could transmit Histone deacetylase 1 (HDAC1) and KRAS siRNAs (against a G12D mutant KRAS gene) to Panc-1 cancer cells for synergistic PTT and gene silencing therapy. The photothermal conversion effect of MoS_2 NSs with NIR laser irradiation and the inactivation of HDAC1 and KRAS genes thus caused obvious cell apoptosis, inhibited migration, and induced cell cycle arrest in treated cancer cell group. *In vivo* anti-tumor experiments testified that the growth of tumors in FA/MoS_2/siRNA (HDAC1 + KRAS) plus laser irradiation was significantly suppressed, illustrating that PTT combined with gene therapy has prominent anticancer efficacy.

4.3. Combination of PTT with chemotherapy

As one of the most commonly used cancer treatments in clinic, chemotherapy employs drugs to specifically inhibit cancer cells [124–126]. However, the existing drugs used in chemotherapy have the shortcomings such as short circulation period, insufficient accumulation at tumor sites, instability and low selectivity, which not only limit the therapeutic effect, but may even produce high toxicity to normal tissues and organs [127–131]. Therefore, the design of stimulus-responsive drug nanocarriers to control drug release in space/time while simultaneously enhancing drug uptake by cancer cells is an innovative strategy to improve the chemotherapy effect.

Recently, different types of drug delivery platforms based on nanomaterials, such as pH, temperature and magnetic responsive drug release, have been developed rapidly [132–136]. Among them, 2D TMCs nanomaterials could be employed as ideal candidates for effective thermally responsive drug-loading nanocarriers mediated by NIR laser because of their extraordinary surface area and strong NIR absorption. As reported, Liu *et al.* first discovered that 2D TMCs nanomaterials with appropriate surface modification could be introduced as an attractive class of 2D nanocarriers for the highly efficient loading of the chemotherapy drugs such as doxorubicin (DOX) and 7-ethyl-10-hydroxycamptothecin (SN38) (Fig. 10) [137]. PEGylation MoS_2 (MoS_2-PEG) was selected as a typical example, and experimental results displayed that the drug loading capacity of MoS_2-PEG with a large surface-area-to-mass ratio was significantly higher than that of PEGylated graphene oxide. As expected, *in vitro* and *in vivo* results validated the prominent synergistic anti-tumor effect of MoS_2-PEG-FA/DOX. Similarly, Zhao *et al.* prepared chitosan (CS) coated MoS_2 (MoS_2-CS) NSs as drug nanocarriers [23]. After loaded with DOX molecules, an effective NIR stimulus-responsive nano-system for synergistic chemotherapy and PTT was achieved. *In vitro* and *in vivo* tumor treatment studies demonstrated that MoS_2-CS-DOX + NIR group had a better pancreatic cancer therapeutic effect associated with the synergistic NIR-induced hyperthermia and heat-stimulated chemotherapy drugs release than either chemotherapy or PTT alone.

To improve the efficacy of combination therapy, Yang *et al.* prepared mesoporous silica (MS) coated, iron oxide (IO) decorated and PEG modified WS_2 NSs (WS_2-IO@MS-PEG) [138]. In this nanoplatform, WS_2-IO@MS-PEG was further loaded with DOX to acquire WS_2-IO@MS-PEG/DOX, and a remarkable cancer-killing effect with the addition of NIR laser irradiation was observed. *In vivo* studies showed that the tumor growth in the combined PTT with chemotherapy group (WS_2-IO@MS-PEG/DOX with NIR laser irradiation) was substantially inhibited, exhibiting much superior performance than single therapy. The reason for this highly synergistic effect is that the mild hyperthermia could improve cell membrane permeability, thereby enhancing the intracellular delivery of drugs. Simultaneously, NIR triggered the drugs release from WS_2-IO@MS-PEG/DOX especially under the condition of intracellular acidity, which further enhanced the killing effect of chemotherapy.

4.4. Combination of PTT with PDT

Unlike PTT, which involves a heat conduction process, PDT typically utilizes photosensitizer molecules to produce large amounts of singlet oxygen ($^1O_2$) under laser irradiation, thus causing irreversible damage to cancer cells [139,140]. The efficient generation of $^1O_2$ requires the optimal combination of three pivotal factors: light, photosensitizer, and oxygen. Unfortunately, the tumor microenvironment is typically hypoxic, which results in the low $^1O_2$ production and consequently limits the effectiveness of PDT. To address this thorny problem, researchers have tried to combine PDT with PTT for enhanced cancer treatment because hyperthermia may enhance the intratumoral blood flow, thereby improving the hypoxia at the tumor site and strengthening the efficiency of PDT.

In recent years, 2D TMCs nanomaterials with unique structural features and excellent photothermal conversion efficiency have been reported as simple and powerful nanoplatforms for synergistic PTT/PDT therapy. For example, Zhao *et al.* first employed WS_2 NSs as nanocarriers to load photosensitizer methylene blue (MB) molecules for combined PTT and PDT in cancer treatment [91]. They found that the generation of $^1O_2$ could be well controlled by regulating the release behavior of MB from WS_2 NSs with NIR irradiation. This is because WS_2 NSs have quenching ability, and the adsorption of MB on the surface of WS_2 NSs could effectively restrain the generation of $^1O_2$. In the case of NIR irradiation, hyperthermia could disturb the interaction between MB and WS_2, causing the release of MB from the surface of WS_2, thus realizing the effective generation of $^1O_2$ for PDT. This interesting phenomenon indicated the potential of BSA-WS_2@MB nanocomposites to be intelligent nanoplatforms for controlled $^1O_2$ generation. *In vitro* results clearly confirmed that PDT combined with PTT is more effective in killing cancer cells than individual PDT and PTT.

Subsequently, Liu *et al.* first demonstrated the synergistic treatment of PTT and PDT based on 2D TMCs *in vivo* (Fig. 11) [141]. In this work, photosensitizers chlorin e6 (Ce6)-loaded MoS_2-PEG (MoS_2-PEG/Ce6) NSs were designed for combined PTT and PDT. *In vitro* experiments revealed that MoS_2-PEG/Ce6 could remarkably improve the intracellular delivery of Ce6 and thus dramatically kill cancer cells with laser irradiation. This could be ascribed to the mild hyperthermia that could improve the cell membrane permeability. After PEG-MoS_2/Ce6 were intravenously injected into 4T1 tumor-bearing mice, a remarkable inhibition of tumor growth was revealed under additional laser irradiation.

4.5. Combination of PTT with RT

As an important antitumor modality, RT employs ionizing radiation to destroy the DNA of cancer cells or induce oxidative stress to achieve cancer treatment [142,143]. However, RT has also encountered a series of bottlenecks, such as the damage of normal tissues, resistance to radiation (especially for tumors that have undergone multiple rounds of treatment), and the low efficiency for hypoxic tumor microenvironments. Fortunately, hyperthermia from the PTT can increase the sensitivity of RT by increasing the intratumoral blood flow and alleviating hypoxia at the tumor site. Moreover, PTT can efficiently kill cancer cells insensitive to RT. Hence, the combination of PTT and RT might be an effective strategy to overcome the existing limitations of RT alone.

Owing to their good X-ray attenuation and intrinsic NIR absorption ability, 2D TMCs with a high Z atomic number (such

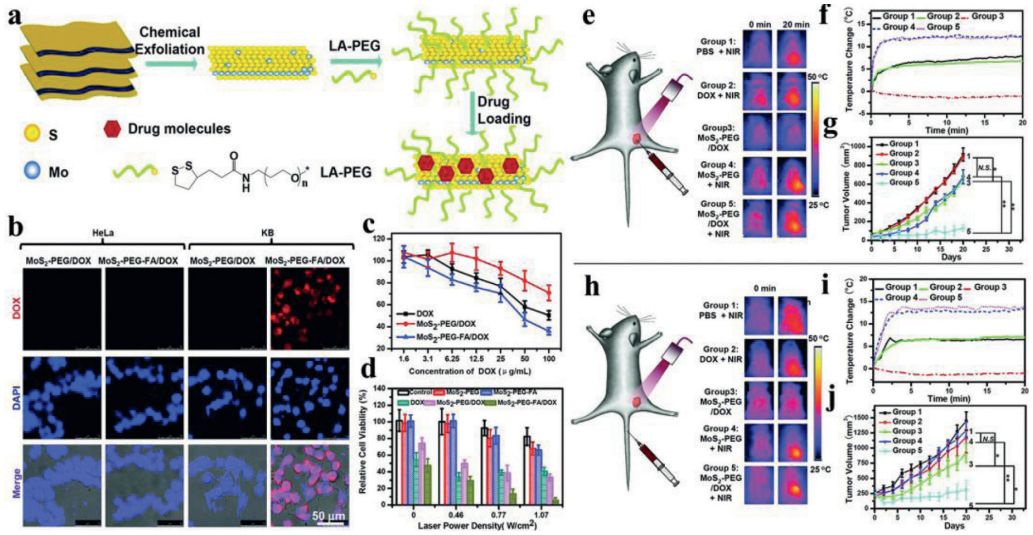

Fig. 10. (a) Schematic illustration of the fabrication process of MoS_2-PEG and subsequent drug loading. (b) Confocal fluorescence images of HeLa and KB cells after incubation with MoS_2-PEG/DOX and MoS_2-PEG-FA/DOX for 1 h. (c) Relative viabilities of KB cells after incubation with free DOX, MoS_2-PEG/DOX and MoS_2-PEG-FA/DOX at different concentrations. (d) Relative viabilities of KB cells after various treatments. (e) The combination therapy based on intratumorly injected MoS_2-PEG/DOX and IR thermal images of 4T1 tumor-bearing mice, recorded by an IR camera. (f) Temperature changes of tumors monitored by an IR thermal camera in different groups during laser irradiation. (g) Tumor volume growth curves of different groups of mice after various treatments. (h) The combination therapy based on intravenously injected MoS_2-PEG/DOX and IR thermal images of 4T1 tumor-bearing mice, recorded by an IR camera. (i) Temperature changes of tumors monitored by an IR thermal camera in different groups during laser irradiation. (j) Tumor volume growth curves of different groups of mice after various treatments. Reproduced with permission [137]. Copyright 2014, Wiley-VCH Verlag GmbH & Co. KGaA, Weinheim.

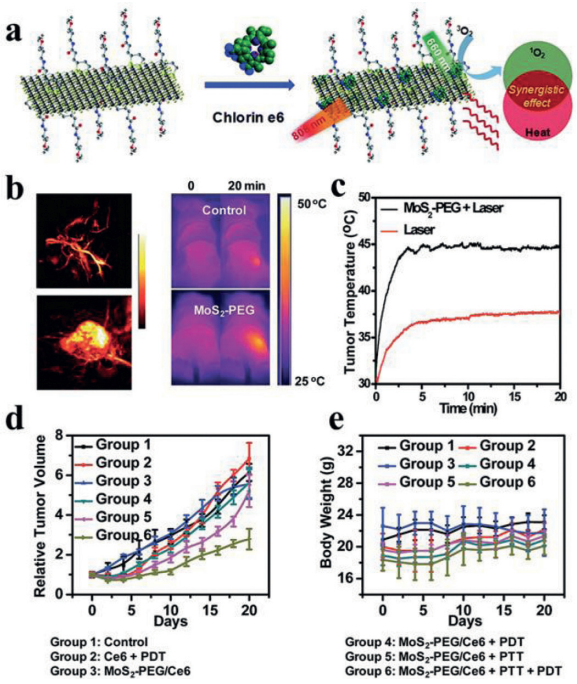

Fig. 11. (a) Scheme illustration of MoS_2-PEG/Ce6 NSs for Ce6 loading and combined photothermal and photodynamic therapy. (b) Photoacoustic images and (c) IR thermal images of tumors in mice. (d) Surface temperature changes of tumors monitored by an IR thermal camera during laser irradiation. (e) Relative tumor volume curves of different groups of mice after various treatments. (f) Average body weight of mice after various treatments. Reproduced with permission [141]. Copyright 2014, Royal Society of Chemistry.

as WS_2, Bi_2S_3 and Bi_2Se_3) have been employed in the combination of PTT and RT. As reported, Liu *et al.* developed Gd^{3+}-doped WS_2 (WS_2:Gd^{3+}) NSs and modified them with PEG to generate WS_2:Gd-PEG as photothermal treatment agents and radiosensitizers for the efficient combination of PTT and RT [81]. *In vitro* and *in vivo* anti-tumor results displayed that the synergistic PTT and RT produced by WS_2: Gd-PEG with NIR and X-ray radiation could realize significant synergistic destruction effect on cancer cells. Subsequently, Liu *et al.* continued to prepare $FeSe_2$ decorated Bi_2Se_3 ($FeSe_2$/Bi_2Se_3) NSs and further functionalized them with PEG to construct a nanoplatform for synergistic PTT and RT [103]. The prepared $FeSe_2$/Bi_2Se_3-PEG nanomaterials were labeled with radioisotope ^{64}Cu to fabricate ^{64}Cu-$FeSe_2$/Bi_2Se_3-PEG with strong NIR and X-ray absorption properties for high-efficiency cancer treatment. The effective and specific anti-tumor efficacy of combinatorial PTT and RT was confirmed in the 4T1 cells and 4T1 tumor-bearing mice treated with $FeSe_2$/Bi_2Se_3-PEG + X-ray + NIR. Similarly, Chen *et al.* constructed novel and multifunctional MoS_2/Bi_2S_3-PEG (MBP) NSs to realize combined PTT and RT (Figs. 12a-e) [93]. The MoS_2 nanosheet and surface-decorated Bi_2S_3 NPs endowed MBP with prominent PTT efficiency and outstanding radiation enhancement effect during RT respectively. After intravenous injection of 2D MBP nanocomposites, significantly suppressed tumor growth was observed and no obvious tumor recurrence was revealed during the whole treatment, which confirms the synergistic anti-tumor efficiency of the 2D MBP nanocomposites.

Internal radioisotope therapy (RIT) is considered as an alternative to external-beam RT (EBRT) which absorbs external X-ray beams. Chao *et al.* fabricated PEG functionalized WS_2 NSs and labeled them with radioisotope by using a chelator-free strategy to acquire ^{188}Re-WS_2-PEG with high radiolabeling stability (Figs. 12f-i) [144]. *In vitro* studies showed that ^{188}Re-WS_2-PEG displayed significantly enhanced damage to cancer cells than free ^{188}Re without external X-ray irradiation. This is because ^{188}Re serves as a radioemitter and WS_2 serves as a radiosensitizer; therefore ^{188}Re-WS_2-PEG is able to effectively emit β-ray and γ-ray for cancer treatment. Subsequently, a 4T1 tumor model was established to evaluate the synergistic therapeutic effect of ^{188}Re-WS_2-PEG *in vivo*. The results showed that the tumors of 4T1 tumor-bear mice treated with ^{188}Re-WS_2-PEG were completely eliminated after introducing laser irradiation, demonstrating that ^{188}Re-WS_2-PEG could effectively combine PTT and RT to achieve synergistic anti-cancer effect. To sum up, 2D TMCs composites with ex-

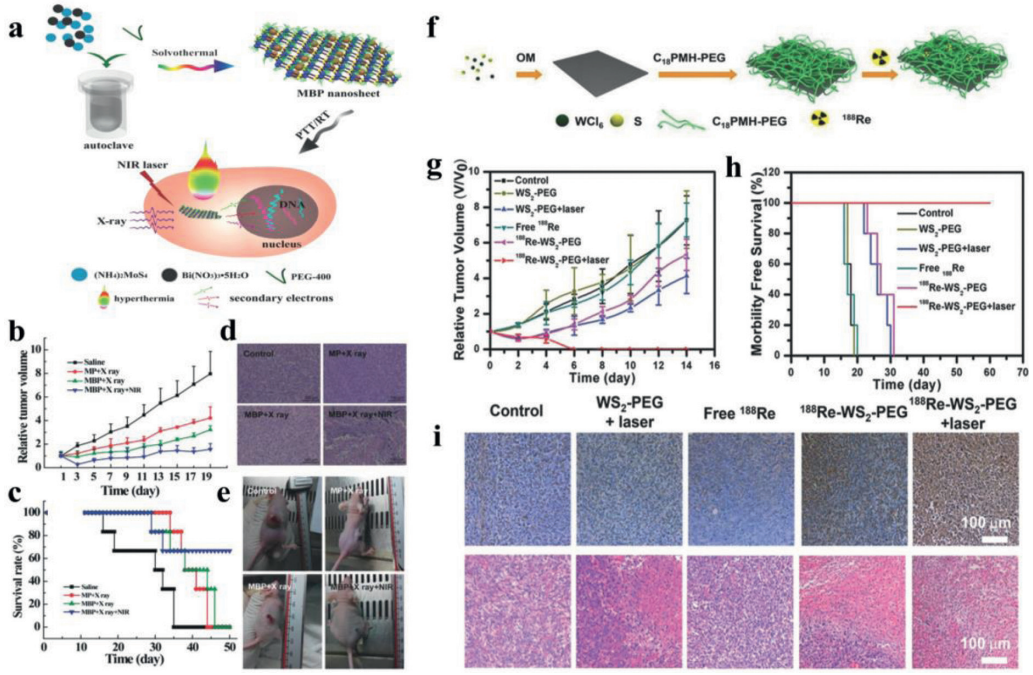

Fig. 12. (a) Schematic illustration of the solvothermal synthesis of MBP NSs and combined PTT and RT. (b) Tumor growth profiles of 4T1 tumors after various treatments. (c) Tumor bearing 4T1 mice survival rates as a function of time post different treatments. (d) H&E staining of tumor sections after different treatments. (e) Representative photos of 4T1 tumor bearing mice on day 28 post various treatments. Reproduced with permission [93]. Copyright 2015, Wiley-VCH Verlag GmbH & Co. KGaA, Weinheim. (f) Schematic illustration of the synthesis and modification of WS_2 NSs and radiolabeling of ^{188}Re. (g) Relative tumor volumes and (h) survival rates of mice after different treatments. (i) Representative TUNEL and (j) H&E stained tumor slices from six groups. Reproduced with permission [144]. Copyright 2016, Wiley-VCH Verlag GmbH & Co. KGaA, Weinheim.

Table 2
Various 2D TMCs nanomaterials with their applications and functions.

Applications	Materials	Assisted molecule	Synthesis methods	Function	Ref.
Biological imaging	Gd^{3+}-doped $MoSe_2$	$GdCl_3$	Solvothermal method	Gd ion doping for MR imaging	[86]
	MoS_2/Bi_2S_3	Bi_2S_3	Solvothermal method	Bi_2S_3 for CT imaging	[93]
	MoS_2	mPEG-co-PPyr	Solvent-assisted exfoliation	Shell structure for PA imaging	[98]
	^{64}Cu-$FeSe_2/Bi_2Se_3$	Bi_2Se_3, radioisotope ^{64}Cu	Solvothermal method	Composite-nanostructures for MR/CT/PA/PET imaging	[103]
Cancer treatment	$CuFe_2S_3$	PEG	Solvothermal method	High temperature for PTT	[78]
	MoS_2	LA-PEG, PEI, siRNA	Chemical-assisted intercalation and exfoliation	High temperature and genetic materials as therapeutic drugs for combination of PTT with gene therapy	[121]
	MoS_2	CS, DOX	Solvent-assisted exfoliation	High temperature and chemotherapy drugs for combination of PTT with gene therapy	[23]
	WS_2	BSA, MB	Chemical-assisted intercalation and exfoliation	High temperature and photosensitive drugs for combination of PTT with PDT	[91]
	WS_2	PEG, ^{188}Re	Solvent-assisted exfoliation	High temperature and excellent radiosensitizing effect for combination of PTT with PDT	[144]

cellent radiosensitizing effect, desirable photothermal performance and good biocompatibility show great promise in future clinical applications.

5. Conclusions and prospects

As emerging candidates in the field of nano-biomedicine, 2D TMCs with unique structural features, tunable electronic band structure and abundant chemical element composition are of great significance to the cancer diagnosis and treatment. Up to now, a series of TMCs NSs have acquired substantial success in the field of imaging-guided cancer treatment. In this review, we detailedly summarized the synthesis methods of 2D TMCs nanomaterials and systematically discussed their application in biological imaging and cancer treatment (Table 2). Although 2D TMCs hold great promise as ideal and promising nanomaterials for cancer diagnosis and treatment, there are still some challenges need to be addressed before their translation into clinical application.

First of all, current synthesis methods still have some limitations. For example, the size, shape and thickness of 2D TMCs nanomaterials would affect their diagnostic performance and treatment efficiency. However, neither the chemical method and the electrochemical intercalation method nor liquid exfoliation can effectively control the size and thickness of 2D TMCs nanomaterials. With the rapid development of chemical synthesis, the hydrothermal/solvothermal method is expected to be a feasible approach to prepare NSs with controlled and desirable structure for better cancer therapy. Nevertheless, it is still to further improve the current

hydrothermal/solvothermal method so as to obtain 2D TMCs with well-shaped morphology and tunable composition.

Secondly, the establishment of desirable surface functionalization technology to synthesize suitable and nontoxic 2D TMCs nanomaterials is of great significance in the practical cancer therapeutic applications. For the surface functionalization of TMC NSs, good biocompatibility and hydrophilic surfaces are required for 2D TMCs stably dispersed in water and various physiological solutions, and active functional groups on the surface of 2D TMCs are beneficial to subsequent biocoupling with a variety of biomolecules to target specific sites. Although 2D TMCs nanomaterials functionalized by thiol chemistry or physical absorption have been reported, the instability in complicated physiological surroundings still remains a problem due to their susceptibility to different pH, intracellular reducing agent or temperature. Thus, more efforts are needed to explore appropriate, nontoxic and effective functionalization strategies to prepare functionalized TMCs nanomaterials with excellent stability for cancer treatment.

Thirdly, the hyperpyrexia mediated by 2D TMCs nanomaterials may also activate the normal cells around the tumor site and cause inevitable damage to normal cells and tissues. Therefore, it is of great significance to precisely control the heating position and heating rate of 2D TMCs nanomaterials in cancer treatment. One possible solution is to develop low-temperature PTT to induce tumor cell death, thus avoiding this problem.

Fourthly, although 2D TMCs nanomaterials can be employed to construct multimodal imaging and therapeutic nanoplatforms by doping certain elements or integrating with therapeutic approaches, however, this multimodal nanoplatform may affect the performance of each approach. Therefore, when constructing a nanosystem, the loading ratio of drugs or imaging contrast agents, and the degree of loss of biological activity during delivery to treatment sites need to be considered. Moreover, reasonable evaluation criteria should be established to balance the functional properties and complexity.

Fifthly, although the *in vivo* degradation and metabolism of most 2D TMCs nanomaterials have been proved by some studies, the toxicity of the entire class of 2D TMCs has not been assessed and compared. Moreover, the research on the long-term efficacy and the mechanism of toxicity *in vivo* still remains inadequate. Therefore, with the continuous increase of imaging contrast agents and therapeutic agents based on nanomaterials, further and more in-depth studies of the long-term biosafety and immunotoxicity induced by 2D TMCs nanomaterials *in vivo* is of great importance. Further clinical research can be conducted only after the biological safety of 2D TMCs nanomaterials has been demonstrated.

Finally, there are still some issues to consider before practical biomedical applications, such as the method and dose of administration. In terms of administration method, current cancer treatment studies generally involve injecting therapeutic agents intravenously into the body. Therefore, attention should be paid to the stability of 2D TMCs nanomaterials in blood. Regarding the dosage of 2D TMCs nanomaterials, it is also necessary to notice whether they will cause significant toxicity *in vivo*. Practical biomedical applications of TMCs nanomaterials with 2D structure in the diagnosis and treatment of cancer will be realized when these issues are fully considered and properly addressed.

Undoubtedly, some remarkable advances in the preparation of TMCs NSs and their applications in the diagnosis and treatment of cancer have been achieved. Despite some unsolved questions, we still believe that 2D TMCs nanomaterials with satisfactory functionalities and wholesome biosafety profiles will move towards future clinical application. We hope that this review will inspire more efforts to the preparation and biomedicine applications of TMCs NSs, and we totally convinced that more encouraging results will be obtained in the near future.

Declaration of competing interest

The authors declare that they have no known competing financial interests or personal relationships that could have appeared to influence the work reported in this paper.

Acknowledgments

This work was supported by the National Natural Science Foundation of China (NSFC, Nos. 21971007, 21521005, 51902012), Beijing Natural Science Foundation (No. 2212044), and the Fundamental Research Funds for the Central Universities (Nos. XK1802-6, XK1803-05).

References

[1] C. Cui, J. Yang, X. Li, et al., Mol. Cancer 19 (2020) 58.
[2] Y. Qi, H. Min, A. Mujeeb, et al., ACS Appl. Mater. Interfaces 10 (2018) 6972–6981.
[3] X. Wang, G. Ramamurthy, A.A. Shirke, et al., Cancer Res. 80 (2020) 156–162.
[4] Y. Yuan, Z. Gu, C. Yao, D. Luo, D. Yang, Small 15 (2019) 1900172.
[5] W.K. Peitsch, I. Hofmann, J. Bulkescher, et al., J. Invest. Dermatol. 125 (2005) 761–774.
[6] T. Hu, X. Mei, Y. Wang, et al., Sci. Bull. 64 (2019) 1707–1727.
[7] X. Wang, H.M. Cheng, X.W. Gao, et al., Chin. Chem. Lett. 30 (2019) 919–923.
[8] D. Yan, J. Lu, L. Chen, et al., Chem. Commun. 46 (2010) 5912–5914.
[9] X. Ji, N. Kong, J. Wang, et al., Adv. Mater. 30 (2018) 1803031.
[10] M. Qiu, A. Singh, D. Wang, et al., Nano Today 25 (2019) 135–155.
[11] W. Tao, X. Ji, X. Zhu, et al., Adv. Mater. 30 (2018) 1802061.
[12] X. Jiang, S. Zhang, F. Ren, et al., ACS Nano 11 (2017) 5633–5645.
[13] W. Zhen, Y. Liu, L. Lin, et al., Angew. Chem. Int. Ed. 57 (2018) 10309–10313.
[14] J. Azadmanjiri, V.K. Srivastava, P. Kumar, et al., Appl. Mater. Today 19 (2020) 100600.
[15] S. Manzeli, D. Ovchinnikov, D. Pasquier, O.V. Yazyev, A. Kis, Nat. Rev. Mater. 2 (2017) 17033.
[16] Q. Liang, J. Gou, Arramel, et al., Nano Res. 13 (2020) 3439–3444.
[17] Q. Fu, J. Han, X. Wang, et al., Adv. Mater. 33 (2021) 1907818.
[18] T. Kim, D. Kang, Y. Lee, et al., Adv. Funct. Mater. 30 (2020) 2004140.
[19] L. Yuwen, Y. Sun, G. Tan, et al., Nanoscale 10 (2018) 16711–16720.
[20] W. Choi, N. Choudhary, G.H. Han, et al., Mater. Today 20 (2017) 116–130.
[21] L. Gong, L. Yan, R. Zhou, et al., J. Mater. Chem. B 5 (2017) 1873–1895.
[22] H. Chen, T. Liu, Z. Su, L. Shang, G. Wei, Nanoscale Horiz 3 (2018) 74–89.
[23] Y. Zhang, Y. Yao, M.G. Sendeku, et al., Adv. Mater. 31 (2019) 1901694.
[24] X. Chia, M. Pumera, Chem. Soc. Rev. 47 (2018) 5602–5613.
[25] T. Chowdhury, E.C. Sadler, T.J. Kempa, Chem. Rev. 120 (2020) 12563–12591.
[26] S. Zhu, L. Gong, J. Xie, Z. Gu, Y. Zhao, Small Methods 1 (2017) 1700220.
[27] Y. Wang, M. Qiu, M. Won, et al., Coord. Chem. Rev. 400 (2019) 213041.
[28] H. Zhang, G. Chen, B. Yu, Y. Shen, H. Cong, ACS Appl. Bio Mater. 2 (2019) 3870–3876.
[29] J. Chen, C. Ning, Z. Zhou, et al., Prog. Mater. Sci. 99 (2019) 1–26.
[30] Z. Lei, W. Zhu, S. Xu, et al., ACS Appl. Mater. Interfaces 8 (2016) 20900–20908.
[31] B. Ding, C. Yu, C. Li, et al., Nanoscale 9 (2017) 16937–16949.
[32] Y. Zhu, Y. Wang, G.R. Williams, et al., Adv. Sci. 7 (2020) 2000272.
[33] S. Wang, J. Zhao, H. Yang, et al., Acta Biomater 58 (2017) 442–454.
[34] L. Cheng, J. Liu, X. Gu, et al., Adv. Mater. 26 (2014) 1886–1893.
[35] J. Chen, C. Liu, D. Hu, et al., Adv. Funct. Mater. 26 (2016) 8715–8725.
[36] V. Agarwal, K. Chatterjee, Nanoscale 10 (2018) 16365.
[37] Q. Yang, Nano Life 6 (2016) 1642008.
[38] K.S. Novoselov, A.K. Geim, S.V. Morozov, Science 306 (2016) 666–669.
[39] C. Chang, W. Chen, Y. Chen, et al., Acta Phys. Chim. Sin. 37 (2021) 2108017.
[40] H. Huang, J. Zha, S. Li, C. Tan, Chin. Chem. Lett. 33 (2022) 163–176.
[41] C. Tan, L. Zhao, P. Yu, et al., Angew. Chem. Int. Ed. 56 (2017) 7842–7846.
[42] F. Lei, Y. Sun, K. Liu, et al., J. Am. Chem. Soc. 136 (2014) 6826–6829.
[43] C. Tan, H. Zhang, Nat. Commun. 6 (2015) 7873.
[44] H. Duan, N. Yan, R. Yu, et al., Nat. Commun. 5 (2014) 3093.
[45] X. Zhang, Z. Lai, C. Tan, H. Zhang, Angew. Chem. Int. Ed. 55 (2016) 8816–8838.
[46] K.S. Novoselov, D. Jiang, F. Schedin, et al., Proc. Natl. Acad. Sci. USA 102 (2005) 10451–10453.
[47] C. Huo, Z. Yan, X. Song, H. Zeng, Sci. Bull. 60 (2015) 1994–2008.
[48] Y.H. Ma, W.T. Dou, Y.F. Pan, et al., Adv. Mater. 29 (2017) 1604253.
[49] J. Shen, Y. Pei, M. Wang, et al., Adv. Mater. Interfaces 4 (2017) 1600847.
[50] K. Kalantar-zadeh, J.Z. Ou, T. Daeneke, et al., Adv. Funct. Mater. 25 (2015) 5086–5099.
[51] G.R. Bhimanapati, Z. Lin, V. Meunier, et al., ACS Nano 9 (2015) 11509–11539.
[52] C.N.R. Rao, H.S.S.R. Matte, U. Maitra, Angew. Chem. Int. Ed. 52 (2013) 13162–13185.
[53] J.N. Coleman, M. Lotya, A. O'Neill, et al., Science 331 (2011) 568–571.
[54] C. Altavilla, M. Sarno, P. Ciambelli, Chem. Mater. 23 (2011) 3879–3885.
[55] W. Yin, L. Yan, J. Yu, et al., ACS Nano 8 (2014) 6922–6933.
[56] M.M. Bernal, L. Álvarez, E. Giovanelli, et al., 2D Mater. 3 (2016) 035014.
[57] J.I. Paredes, S. Villar-Rodil, Nanoscale 8 (2016) 15389–15413.
[58] G. Yang, C. Zhu, D. Du, J. Zhu, Y. Lin, Nanoscale 7 (2015) 14217–14231.

[59] S. Karunakaran, S. Pandit, B. Basu, M. De, J. Am. Chem. Soc. 140 (2018) 12634–12644.
[60] C. Zhang, D.F. Hu, J.W. Xu, et al., ACS Nano 12 (2018) 12347–12356.
[61] E. Benavente, M.A. Santa Ana, F. Mendizabal, G. Gonzalez, Coord. Chem. Rev. 224 (2002) 87–109.
[62] S.S. Chou, B. Kaehr, J. Kim, et al., Angew. Chem. Int. Ed. 52 (2013) 4160–4164.
[63] Q. Zhang, L. Mei, X. Cao, Y. Tang, Z. Zeng, J. Mater. Chem. A 8 (2020) 15417–15444.
[64] J. Zheng, H. Zhang, S. Dong, et al., Nat. Commun. 5 (2014) 2995.
[65] E.D. Grayfer, M.N. Kozlova, V.E. Fedorov, Adv. Colloid Interface Sci. 245 (2017) 40–61.
[66] F. Yang, K. Wang, P. Hu, et al., Appl. Surf. Sci. 525 (2020) 145867.
[67] G.S. Bang, K.W. Nam, J.Y. Kim, et al., ACS Appl. Mater. Interfaces 6 (2014) 7084–7089.
[68] S. Fan, H.Du X.Z, et al., J. Phys. Chem. C 121 (2017) 13599–13605.
[69] Per Joensen, R.F. Frindt, S. Roy Morrison, Mat. Res. Bull. 21 (1986) 457–461.
[70] E.L.K. Chng, Z. Sofer, M. Pumera, Nanoscale 6 (2014) 14412–14418.
[71] A. Anto Jeffery, C. Nethravathi, M. Rajamathi, J. Phys. Chem. C 118 (2014) 1386–1396.
[72] Z. Zeng, T. Sun, J. Zhu, et al., Angew. Chem. Int. Ed. 51 (2012) 9052–9056.
[73] X. Wang, X. Shen, Z. Wang, R. Yu, L. Chen, ACS Nano 8 (2014) 11394–11400.
[74] X. Guo, Y. Wang, F. Wu, Y. Ni, S. Kokot, Analyst 140 (2015) 1119–1126.
[75] S. Wang, Y. Chen, X. Li, et al., Adv. Mater. 27 (2015) 7117–7122.
[76] J. Wu, G.R. Williams, Y. Zhu, et al., Biomaterials 273 (2021) 120807.
[77] J. Wu, S. Zhang, X. Mei, et al., ACS Appl. Mater. Interfaces 12 (2020) 48310–48320.
[78] S. Wang, T. Hu, G. Wang, et al., Chem. Eng. J. 419 (2021) 129458.
[79] S. Shen, Y. Chao, Z. Dong, et al., Adv. Funct. Mater. 27 (2017) 1700250.
[80] X. Qian, S. Shen, T. Liu, L. Cheng, Z. Liu, Nanoscale 7 (2015) 6380–6387.
[81] L. Cheng, C. Yuan, S. Shen, et al., ACS Nano 9 (2015) 11090–11101.
[82] C. Tan, X. Cao, X.J. Wu, et al., Chem. Rev. 117 (2017) 6225–6331.
[83] Y. Wu, M.R.K. Ali, K. Chen, N. Fang, M.A. El-Sayed, Nano Today 24 (2019) 120–140.
[84] V.H.F. de Abreu, K.K. Peck, N.M. Petrovich-Brennan, K.M. Woo, A.I. Holodny, Radiology 281 (2016) 876–883.
[85] K. Yang, G. Yang, L. Chen, et al., Biomaterials 38 (2015) 1–9.
[86] J. Pan, X. Zhu, X. Chen, Y. Zhao, J. Liu, Biomater. Sci. 6 (2018) 372–387.
[87] Y. Cui, J. Yang, Q. Zhou, et al., ACS Appl. Mater. Interfaces 9 (2017) 5900–5906.
[88] L. Liu, J. Wang, X. Tan, et al., J. Mater. Chem. B 5 (2017) 2286–2296.
[89] T. Liu, S. Shi, C. Liang, et al., ACS Nano 9 (2015) 950–960.
[90] X.Z. Cui, Z.G. Zhou, Y. Yang, et al., Chin. Chem. Lett. 26 (2015) 749–754.
[91] Y. Yong, L. Zhou, Z. Gu, et al., Nanoscale 6 (2014) 10394–10403.
[92] B. Geng, H. Qin, F. Zheng, et al., Nanoscale 11 (2019) 7209–7220.
[93] S. Wang, X. Li, Y. Chen, et al., Adv. Mater. 27 (2015) 2775–2782.
[94] Y. Wang, J. Zhao, Z. Chen, et al., Biomaterials 217 (2019) 119282.
[95] J. Weber, P.C. Beard, S.E. Bohndiek, Nat. Methods 13 (2016) 639–650.
[96] L.V. Wang, S. Hu, Science 335 (2012) 1458–1462.
[97] Y. Huang, A.M. Vezeridis, J. Wang, et al., J. Am. Chem. Soc. 139 (2017) 15–18.
[98] H. Lee, H. Kim, T.P. Nguyen, et al., ACS Appl. Mater. Interfaces 8 (2016) 29213–29219.
[99] Z.T. Rosenkrans, C.A. Ferreira, D. Ni, W. Cai, Adv. Healthc. Mater. 10 (2021) 2000690.
[100] D. Ni, E.B. Ehlerding, W. Cai, Angew. Chem. Int. Ed. 58 (2019) 2570–2579.
[101] G. Song, X. Zheng, Y. Wang, et al., ACS Nano 13 (2019) 7750–7758.
[102] J. Yu, W. Yin, X. Zheng, et al., Theranostics 5 (2015) 931–945.
[103] L. Cheng, S. Shen, S. Shi, et al., Adv. Funct. Mater. 26 (2016) 2185–2197.
[104] X. Wang, L. Cheng, Nanoscale 11 (2019) 15685–15708.
[105] H. Xie, Z. Li, Z. Sun, et al., Small 12 (2016) 4136–4145.
[106] S. Liu, X. Pan, H. Liu, Angew. Chem. Int. Ed. 59 (2020) 5890–5900.
[107] D. Zhi, T. Yang, J. O'Hagan, et al., J. Control. Release 325 (2020) 52–71.
[108] H. Wang, J. Yang, P. Cao, et al., Chin. Chem. Lett. 31 (2020) 3015–3026.
[109] Z. Zhou, X. Wang, H. Zhang, et al., Small 17 (2021) 2007486.
[110] Z. Meng, F. Wei, R. Wang, et al., Adv. Mater. 28 (2016) 245–253.
[111] K. Wang, Y. Xiang, W. Pan, et al., Chem. Sci. 11 (2020) 8055–8072.
[112] B.D. Zheng, Q.X. He, X. Li, J. Yoon, J.D. Huang, Coord. Chem. Rev. 426 (2021) 213548.
[113] S. Wang, K. Li, Y. Chen, et al., Biomaterials 39 (2015) 206–217.
[114] C. Fu, L. Tan, X. Ren, et al., Chem. Commun. 54 (2018) 13989–13992.
[115] C. Ruan, C. Liu, H. Hu, et al., Chem. Sci. 10 (2019) 4699–4706.
[116] Z. Wang, X. Zhen, P.K. Upputuri, et al., ACS Nano 13 (2019) 5816–5825.
[117] J. Zhao, C. Zhou, C. Wu, et al., ACS Appl. Mater. Interfaces 10 (2018) 41947–41955.
[118] Z. Zhou, B. Li, C. Shen, et al., Small 16 (2020) 2004173.
[119] D. Cross, J.K. Burmester, Clin. Med. Res. 4 (2006) 218–227.
[120] K. Li, M. Lu, X. Xia, Y. Huang, Chin. Chem. Lett. 32 (2021) 1010–1016.
[121] Z. Kou, R. Yuan, H. Chen, et al., Nanoscale Res. Lett. 9 (2014) 587.
[122] J. Kim, H. Kim, W.J. Kim, Small 12 (2016) 1184–1192.
[123] F. Yin, T. Anderson, N. Panwar, et al., Nanotheranostics 2 (2018) 371–386.
[124] S. Cho, N.G. Min, W. Park, S.H. Kim, D.H. Kim, Adv. Funct. Mater. 29 (2019) 1901384.
[125] M. Hou, Y. Zhong, L. Zhang, et al., Chin. Chem. Lett. 32 (2021) 1055–1060.
[126] Z. Shi, Q. Li, L. Mei, Chin. Chem. Lett. 31 (2020) 1345–1356.
[127] Q. Wu, G. Chen, K. Gong, et al., Matter 1 (2019) 496–512.
[128] P. Li, L. Liu, Q. Lu, et al., ACS Appl. Mater. Interfaces 11 (2019) 5771–5781.
[129] W.D. Yu, G. Sun, J. Li, J. Xu, X. Wang, Cancer Lett 452 (2019) 66–70.
[130] L. Zhou, C. Du, R. Zhang, C. Dong, Chin. Chem. Lett. 32 (2021) 561–564.
[131] Y. Mao, C. Zou, Y. Jiang, D. Fu, Chin. Chem. Lett. 32 (2021) 990–998.
[132] R. Gao, M.S. Kodaimati, D. Yan, Chem. Soc. Rev. 50 (2021) 5564–5589.
[133] R. Gao, X. Fang, D. Yan, J. Mater. Chem. C 7 (2019) 3399–3412.
[134] H. Ma, R. Gao, D. Yan, J. Zhao, M. Wei, J. Mater. Chem. C 1 (2013) 4128–4137.
[135] T.I. Kim, B. Kwon, J. Yoon, et al., ACS Appl. Mater. Interfaces 9 (2017) 7908–7917.
[136] K.S. Huang, C.H. Yang, Y.C. Wang, W.T. Wang, Y.Y. Lu, Pharmaceutics 11 (2019) 212.
[137] T. Liu, C. Wang, X. Gu, et al., Adv. Mater. 26 (2014) 3433–3440.
[138] G. Yang, H. Gong, T. Liu, et al., Biomaterials 60 (2015) 62–71.
[139] F. Wei, T.W. Rees, X. Liao, L. Ji, H. Chao, Coord. Chem. Rev. 432 (2021) 213714.
[140] L. Shen, T. Zhou, Y. Fan, et al., Chin. Chem. Lett. 31 (2020) 1709–1716.
[141] T. Liu, C. Wang, W. Cui, et al., Nanoscale 6 (2014) 11219–11225.
[142] R.M. Pallares, R.J. Abergel, Nano Res. 13 (2020) 2887–2897.
[143] J. Bao, X. Zu, X. Wang, et al., Int. J. Nanomedicine 15 (2020) 7687–7702.
[144] Y. Chao, G. Wang, C. Liang, et al., Small 12 (2016) 3967–3975.